10TH INTERNATIONAL SYMPOSIUM ON PARTICLE IMAGE VELOCIMETRY - PIV13
Delft, The Netherlands, July 1-3, 2013

Vorticity Reorientation in the Near-Tip Region of Rapidly-Accelerating, Finite Aspect-Ratio Plates

Jochen Kriegseis and David E. Rival

Department of Mechanical Engineering, University of Calgary, Calgary, Canada
jochen.kriegseis@ucalgary.ca

ABSTRACT

An investigation into the influence of seemingly analogous plate kinematics (plunge vs. tow) for rapidly accelerating, low aspect-ratio plates has been performed. The data was obtained simultaneously by means of a three-dimensional particle tracking velocimetry (3D-PTV) system together with a six-component force/moment sensor. Despite identical effective shear-layer velocities and effective angles of attack, the force histories are found to vary between the two aforementioned cases (plunge and tow). The LEV formation for both cases was found to be nearly identical during the acceleration phase. However, at the end of acceleration the tow LEV 'rolled-off' the plate. As such, the development of vortex force was also observed to cease once this roll-off process started. In accordance with the literature, the tip vortex has been identified to be an important contributor in the overall force production. Tip-vortex strength as well as its relative positioning to the plate surface influences the instantaneous force. However, in addition to these previous studies it has now been demonstrated, based on a Lamb-vector analysis, that the sensitivity of the resulting vortex-force formation is dependent on the interplay between streamwise vorticity and spanwise (inboard) velocity.

1. INTRODUCTION

As outlined by Dabiri [1], a Lagrangian perspective of the unsteady fluid field about a moving body can elucidate both vortex added mass and circulatory contributions of the time-dependent forces. This is an amelioration over a traditional Eulerian analysis where neither the origin of fluid acceleration nor vorticity from the body surface can be identified. In recent studies Ringuette *et al.* [9] and Kim and Gharib [6] investigated the leading-edge-vortex (LEV) and tip-vortex (TV) development on low aspect ratio (AR) flat plates towed from rest at a 90° angle of attack. It was found that the TV increased the overall drag and that this force increased with lower aspect ratios. In addition, it was observed that the circulation of the LEV decreased at spanwise positions close to the tip.

Recently, Yilmaz and Rockwell [14] presented phase-averaged, three-dimensional flow structures showing the LEV and TV growth on low aspect ratio rectangular and elliptical flat plates undergoing a pitching motion. In their study, LEV eruption was observed, however, less pronounced for the elliptical planform. Similarly, Hartloper *et al.* [4] investigated the strong time-dependent, three-dimensional interaction between both vortical structures (LEV and TV) and showed that significant interaction took place after initial vortex growth. Here the TV grew rapidly and was found to compress the LEV towards the midspan until eruption was observed.

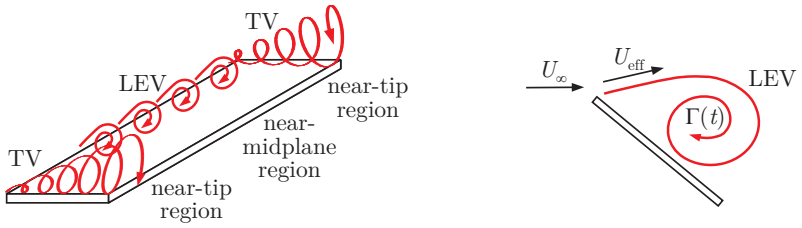

(a) finite aspect ratio plate (b) leading-edge vortex

Figure 1: Sketch of detached vortical structures over a finite aspect ratio plate: (a) distinction of the two-dimensional and three-dimensional regions according to Jardin *et al.* [5]; (b) characteristic velocities for vortex formation and corresponding circulation Γ according to Kriegseis *et al.* [7].

Jardin *et al.* [5] demonstrated that this interaction is limited to the *near-tip region* of the accelerating plate, whereas the flow and thus LEV formation in the *near-midplane region* is largely two-dimensional (see Figure 1(a)). In addition to this distinction, Kriegseis *et al.* [7] observed that for this mid-plane region no history effects from the varying initial conditions were observed in the resulting vortex formation after the rapid acceleration motion was completed. In this study it was furthermore demonstrated that for proper comparison one should non-dimensionalize the vortex dynamics for the varying tow and plunge kinematics using the effective shear-layer velocities U_{eff} rather than freestream (or terminal) velocity U_∞ (see Figure 1(b)). As the feeding shear layer controls growth and therefore strength

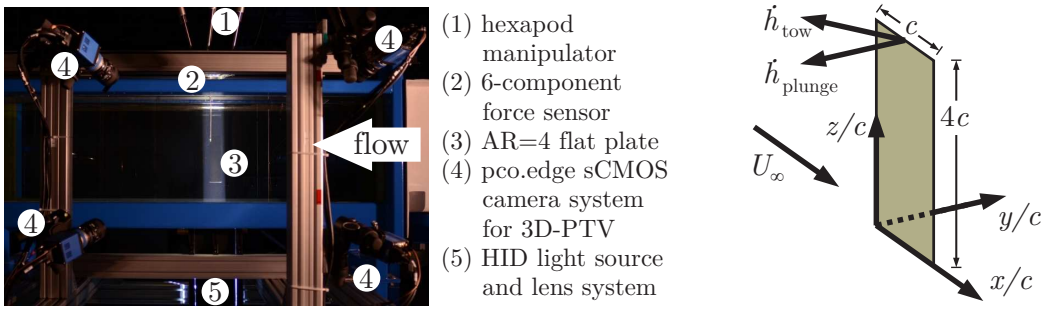

(a) experimental setup in water tunnel

(b) coordinate system

Figure 2: Experimental setup: (a) Water tunnel test section with measurement systems; and (b) AR=4 plate with coordinate system, freestream U_∞ and plunge/tow $\dot{h}$ velocities.

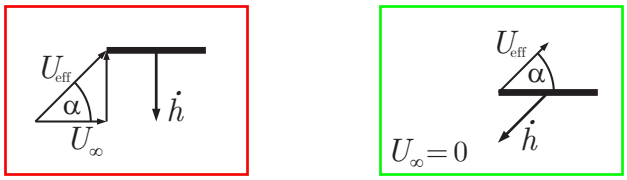

(a) plunging case

(b) towing case

Figure 3: The two plate kinematics used in the study: (a) Plunge to $\alpha_{\text{eff}} = 45^\circ$ with $U_\infty = 0.1$m/s (red); and (b) tow to $\dot{h} = 0.1$m/s with $\alpha_{\text{eff}} = 45^\circ$ (green).

of LEVs through the flux of vorticity-containing mass into the LEV, the advection of circulation into the LEV is a function of the shear layer, with U_{eff} as the relevant characteristic velocity (see e.g. Sattari *et al.* [11]).

In the present study we compare two analogous plate kinematics (plunge vs. tow) with respect to their respective differences in force histories and vortex dynamics. The production and reorientation of vorticity is measured by means of three-dimensional particle tracking velocimetry (3D-PTV). Simultaneously, the resulting forces acting on the plates are measured with a six-component force/moment sensor. The main objective of the present work is to uncover how the discrepancies in the force histories can be explained via differences in the respective vortex dynamics. In particular, the location, size and strength of the vortices will be discussed and the relative contribution of these structures to the resulting lifting forces will then be identified.

2. EXPERIMENTAL AND PROCESSING METHODS

All experiments were conducted in a free-surface water tunnel at the University of Calgary. The plunging and towing motions for an AR=4 plate were controlled by means of a custom hexapod manipulator, which is shown in Figure 2. The three-dimensional Particle Tracking Velocimetry (3D-PTV) technique, as described by Lüthi *et al.* [8], was used to quantify the flow field in proximity of the flat plates. The water tunnel was seeded with neutrally buoyant 100μm silver-coated, hollow-glass spheres with a Stokes number of $Stk \approx 1.2 \times 10^{-3}$. The particles were illuminated by a high-intensity-discharge (HID) light source. A lens system (40mm and 300mm converging lenses) columnated the light to provide a measurement volume with a diameter of 100mm. The plates were painted black to prevent light scattering, and together with the orientation of the light column from below, no digital masking was necessary at the image-processing stage. To track the particles during the experiments, raw images were recorded with four pco.edge sCMOS cameras (chip size 2560×2160pixels, maximal resolution of 2560×1280pixels at 165fps). An ATI Gamma six-component force/moment sensor was mounted between the base of the hexapod and the sting holding the plate so as to record direct force measurements simultaneous to the 3D-PTV measurements.

The plate had a chord length of $c = 50$mm, a span of $4c = 200$mm and a thickness of $t/c = 6\%$. Based on the chord length and freestream velocity U_∞ or the final towing speed $\dot{h}$=0.1m/s, the Reynolds number was set to $Re = 5{,}000$. To identify the influence of plate kinematics on vortex formation and orientation as well as the circulation and overall force history, two plate kinematics were applied to the AR=4 flat plate as sketched in Figure 3.

Superimposed to a freestream velocity $U_\infty = 0.1$m/s, the first case (a) corresponds to a plunge velocity $\dot{h}$ of the plate rapidly increasing to $\dot{h}_{\text{final}} = U_\infty$. This produces an effective plate angle of $\alpha_{\text{eff}} = 45^\circ$ in one convective time $t^*_{\text{eff}} = t\,U_{\text{eff}}/c = 1$ according to a half-cosine curve; see Figure 3(a). In contrast a second case (b) is considered, in which the plate is towed from rest at a constant angle of $\alpha_{\text{eff}} = 45^\circ$; see Figure 3(b). Here the same ramp-up speed as for the plunge case is applied, such that the towing speed of the plate is increased form rest in one convective time to $\dot{h}_{\text{final}} = U_\infty$. For both cases $\dot{h}_{\text{final}}$ is held constant after the initial ramp-up motion to maintain constant U_{eff} and α_{eff} for $1 \leq t^*_{\text{eff}} \leq 2$.

The particle positions and corresponding trajectory information have been determined based on the methods described by Lüthi *et al.* [8]. In a first step, the Lagrangian velocities and (total) velocity derivatives, a_t, of the particles were calculated by differentiation of

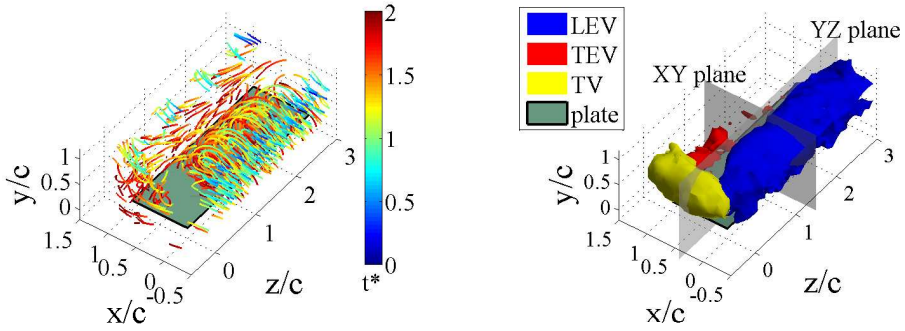

(a) Lagrangian particle tracks

(b) Eulerian iso-surfaces of vorticity ($\omega_i^* = 1.25$)

Figure 4: Exemplary PTV data comparing the Lagrangian and Eulerian representations of the data for the plunge case.

the particle tracks. Local and convective accelerations, a_l and a_c, were subsequently estimated be means of a weighted interpolation of the Lagrangian information from neighbouring particles. The sphere of interest enclosing each particle had an average diameter of $d_s = 5$mm. In a final step all quantities were mapped onto an Eulerian grid with a grid-point spacing of $d_g = d_s = 5$mm.

Based on the method described by Feng *et al.* [2], the relative uncertainty in the particle-track velocity was estimated to be $\delta u/u < \pm 0.01$. An accuracy estimation of the velocity-derivative calculations was performed by comparing the Lagrangian acceleration a_i^t=Du_i/Dt with the sum of the local acceleration a_i^l=$\partial u_i/\partial t$ and convective acceleration a_i^c=$u_j \partial u_i/\partial x_j$ (see Lüthi *et al.* [8]). Calculation of the normalized error σ_a resulting from the acceleration determinations based on

$$\sigma_a = \frac{1}{3} \sum_{i=x,y,z} \frac{|a_i^t - a_i^l - a_i^c|}{|a_i^t| + |a_i^l| + |a_i^c|}, \quad \text{with } \sigma_a \in [0,1], \tag{1}$$

resulted in an uncertainty estimate of $\sigma_a = 0.1$. Some exemplary raw PTV results for the plunge case are shown in Figure 4.

Figure 4(a) exhibits the calculated particle tracks, where the colour coding represents the convective time $t^* = t\,U_{\text{eff}}/c$ elapsed during plate motion. The corresponding Eulerian data was extracted to identify coherent vortical structures, as shown in Figure 4(b) for iso-surfaces of non-dimensional vorticity $\omega_i^* = \omega_i\, c/U_\infty = 1.25$. This image reveals the LEV, TV and some trace of the trailing-edge vortex (TEV). Analysis of all three vorticity components ω_i is performed based on spatial integration across the chosen XY-planes (cp. Figure 4(b)) according to

$$\Gamma_i^* = \frac{c}{U_{\text{eff}}} \iint_{\substack{\text{XY} \\ \text{plane}}} \omega_i \, \mathrm{d}x\mathrm{d}y, \tag{2}$$

where $\Gamma_i^* \mathrel{\hat{=}} \Gamma_x^*, \Gamma_y^*$ and Γ_z^* are based on streamwise, plate-normal and spanwise vorticity components, respectively. The contribution of vorticity (thus circulation) to the lifting force can be distinguished by means of

$$L_i = 2\varepsilon_{ijk}\omega_k u_j, \tag{3a}$$

$$\vec{L} = \vec{u} \times \vec{\omega}, \tag{3b}$$

which is commonly referred to as the *Lamb vector* (see e.g. Wu *et al.* [13]). According to Saffman [10] the magnitude and orientation of $\vec{L}$ correspond to the strength and direction of a vortex force contained in the vortical structure. Therefore, in the present study a positive plate-normal component L_y of the Lamb vector is a contributor to the instantaneous lift force.

As shown by Green [3], the material velocity derivative (Lagrangian acceleration)

$$\frac{\mathrm{D}u_i}{\mathrm{D}t} = \frac{\partial u_i}{\partial t} + u_j \frac{\partial u_i}{\partial x_j} \tag{4}$$

can be decomposed into a rotational and an irrotational component according to

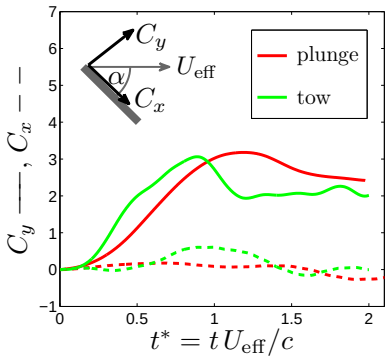

Figure 5: Force-sensor data for the plunging (red) and towing (green) cases; plate-normal force C_y (—) and plate-parallel force C_x (- -).

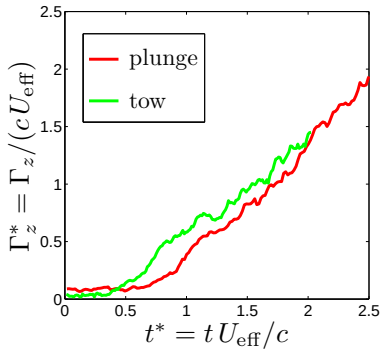

Figure 6: LEV circulation Γ_z^* for the plunging (red) and towing (green) cases in the quasi two-dimensional, near-midplane region ($1 \leq z/c \leq 3$).

$$\frac{\mathrm{D}u_i}{\mathrm{D}t} = \frac{\partial u_i}{\partial t} - 2\varepsilon_{ijk}\omega_k u_j + \frac{\partial}{\partial x_i}\left[\frac{u_j u_j}{2}\right] \tag{5a}$$

$$\frac{\mathrm{D}\vec{u}}{\mathrm{D}t} = \frac{\partial \vec{u}}{\partial t} - \vec{u}\times\vec{\omega} + \nabla\left[\frac{\vec{u}\cdot\vec{u}}{2}\right]. \tag{5b}$$

Therefore, a direct comparison of the the total (Lagrangian) acceleration $\mathrm{D}u_i/\mathrm{D}t$ and and its contribution to the instantaneous lift force (via L_i) can be performed. This quantitative comparison is done at the locations where the XY- and YZ-planes (indicated in Figure 4(b)) cut the LEV and TV, respectively.

3. RESULTS

In order to identify net differences between the two cases (plunge versus tow), the total force results are shown in Figure 5. Normalized according to

$$C_i = \frac{2f_i}{\rho A U_{\text{eff}}^2} \quad \text{with} \quad i = x,y \tag{6}$$

the solid and dashed lines represent the plate-normal and plate-parallel force components C_y and C_x, respectively. Both kinematics produce a rapidly-increasing lift force up to values of $C_y \geq 3$ for $t_{\text{eff}}^* < 1$, with a slightly faster growth for the tow case. In contrast to the plunge case where a higher force is maintained, force drops significantly at $t^* = 1$ for the tow case. Recall that the for both cases the acceleration ceases at $t^* = 1$ such that both kinematics have identical values for α_{eff} and U_{eff} at this time. To understand the differing force histories and particularly the discrepancies for $t^* \geq 1$, the differences in vortex formation and dynamics are discussed in the following.

The LEV-circulation histories Γ_z^* in the near-midplane region (average across $1 \leq z/c \leq 3$) for both cases are compared in Figure 6. Despite varying initial conditions, i.e. attached boundary layer versus a start from rest, both curves have similar slopes for the period of motion, and collapse well for $1 \leq t^* \leq 2$. The salient difference between the curves of near-midplane circulation Γ_z^* and the resulting plate-normal force C_y indicates that a quasi two-dimensional approach oversimplifies the problem. The three main simplifications to be considered are:

(i) The different initial conditions for the plunging and towing kinematics, i.e. $\Gamma_z^*(t^*=0)\big|_{\text{plunge}} = 1$ and $\Gamma_z^*(t^*=0)\big|_{\text{tow}} = 0$;

(ii) the role that the tip vortex plays in the overall force production (see for instance Ringuette *et al.* [9]), which is ignored if a finite aspect-ratio plate (AR=4) is simplified to two-dimensional plate (AR=∞); and

(iii) the time trace of spanwise-averaged circulation covers the spatial information of the flow, i.e. location of the vortices and spatial distribution of vorticity.

In recent studies of varying initial conditions on the resulting circulation history by Weymouth and Triantafyllou [12] and Kriegseis *et al.* [7] it was demonstrated that initial boundary layers are eliminated through cross-annihilation of opposite-signed vorticity layers immediately after the start of rapid acceleration. Consequently, only the varying three-dimensional character, i.e. locations and dimensions of the respective vortical structures cause the different lifting forces, as shown in Figure 5.

Insight into the spatio-temporal evolution of all three vorticity components according to Equation (2) is provided in Figure 7 as a function of span z/c and time t_{eff}^*. Neither streamwise (tip) nor plate-normal vorticity are significant in the mid-plane region, which

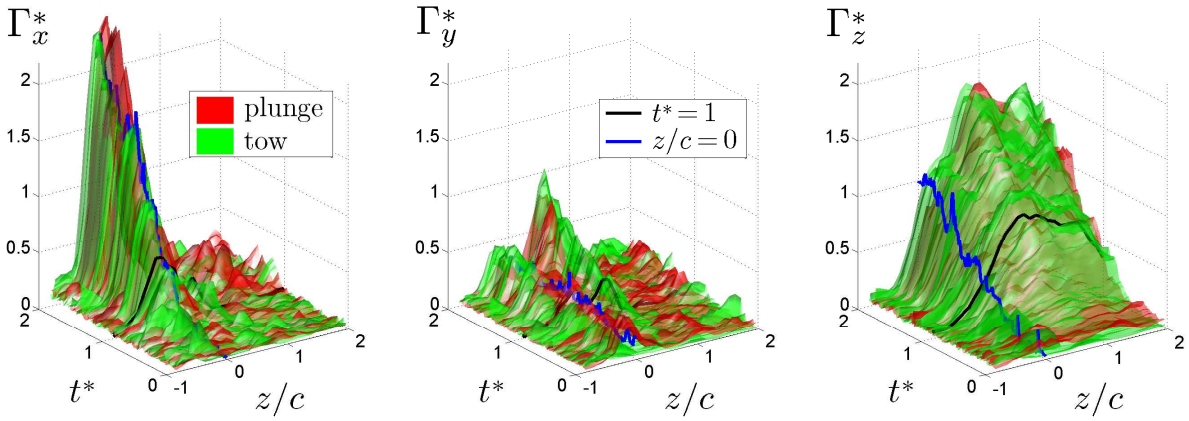

(a) streamwise vorticity ω_x (b) plate-normal vorticity ω_y (c) spanwise vorticity ω_z

Figure 7: Spatio-temporal vorticity distribution as a function of span z/c and time $t^*_{\text{eff}} = tU_{\text{eff}}/c$ for plunging (red) and towing (green) cases; blue and black lines are included to identify $z/c = 0$ (tip location) and $t^* = 1$ (end of acceleration), respectively.

supports the 2D/3D distinction as proposed by Jardin *et al.* [5]. The comparison of Figures 7(a) and 7(c) indicates that both LEV and TV strengths increase simultaneously. The LEV-TV competition, as described by Hartloper *et al.* [4], leads to a deformation of the LEV, which results in the production of plate-normal vorticity as shown in Figure 7(b). However, the identical spanwise distribution and temporal evolution of all vorticity components for both kinematics suggests that location and local distribution of vorticity components dominate the contribution to lifting forces rather than their respective net intensities alone.

In Figure 8 temporal evolution and spatial distributions of spanwise vorticity ω_z^*, plate-normal total acceleration a_z^{t*} and plate-normal component of the Lamb vector (vortex force) are shown for the LEV formation in the near-midplane region (XY-plane) of both cases on top of one another. The corresponding TV formation is exhibited in Figure 9, where instead the streamwise component of vorticity ω_x^* is plotted. Note that both spanwise and streamwise vorticity contribute to the plate-normal component of the Lamb vector

$$L_y = \underbrace{\omega_z u_x}_{\text{LEV}} - \underbrace{\omega_x u_z}_{\text{TV}}, \tag{7}$$

where the first and second right-hand side terms dominate vortex forces of LEV and TV, respectively.

The iso-lines of spanwise vorticity ω_z^* reveal a similar growth of the LEV for both cases (see Figure 8(a)), which reaffirms the insights obtained from the circulation plots of the near-midplane region (see Figure6). However, after the acceleration of the plate stops at $t^* \geq 1$, the tow case LEV 'rolls off' the plate. The acceleration a_y^{t*} of fluid towards the plate remains constant for the plunge case once the acceleration of the plate ceases, as shown in Figure 8(b). In contrast, the domain of accelerated fluid increases significantly for $t^* \geq 1$ and moves towards the plate's leading edge, which results in the observed roll-off. As a result of this adverse vortex motion, the formation of a positive plate-normal vortex force freezes for the tow case, as indicated by iso-lines of L_y^* in Figure 8(c). Since no roll-off occurs for the plunge motion, the LEV vorticity still contributes to a positive vortex force for $t^* \geq 1$. The significant variance in the vortex-force domain leads one to the conclusion that the contribution to lift decays for the tow case once the plate acceleration stops.

The corresponding tip-vortex formation is shown in Figure 9 in a YZ-plane at $x/c = 0.6$ (cp. Figure 4). For both cases the iso-lines of streamwise vorticity ω_x^* demonstrate that the TV forms simultaneously to the LEV, which confirms the findings from the spatio-temporal analysis (see Figure 7). A slight lift-off of the plate can be identified for the tow case, which indicates a less effective contribution to lift (see Kriegseis *et al.* [7]). The iso-line plots of total acceleration do not exhibit any coherent patterns whatsoever, as can be seen in Figure 9(b). This observation suggests that as a first approximation the TV formation, in contrast to the LEV development, demonstrates an approximate solid-body rotation. However, the Lamb-vector iso-lines in Figure 9(c) reveal the formation of a coherent pattern of negative plate-normal vortex force for the towing case. Note that $L_y < 0$ in the TV develops when both positive streamwise vorticity and spanwise velocity occur simultaneously (see Equation (**??**), second term on right-hand side). Since Figure 9(a) shows a similar strength and distribution of streamwise vorticity, it must be concluded that varying magnitudes of inboard velocity ($u_z > 0$) on the suction side is responsible for the development of the negative vortex force $L_y < 0$.

4. CONCLUSIONS

An investigation into the influence of plate kinematics on vortex formation and overall production of a instantaneous lift for rapidly-accelerating, AR=4 plates has been performed for identical U_{eff} and α_{eff}. In particular, the redistribution and reorientation of vorticity $\vec{\omega}$, acceleration $\vec{a}^t = \text{D}u/\text{D}t$ and vortex force $\vec{L} = \vec{u} \times \omega$ in the plate's proximity has been studied. The data was obtained simultaneously by means of a three-dimensional particle tracking velocimetry (3D-PTV) system together with a six-component force/moment sensor. Despite identical terminal values of U_{eff} and α_{eff}, significant variance in the total force histories have been observed for the plunging and

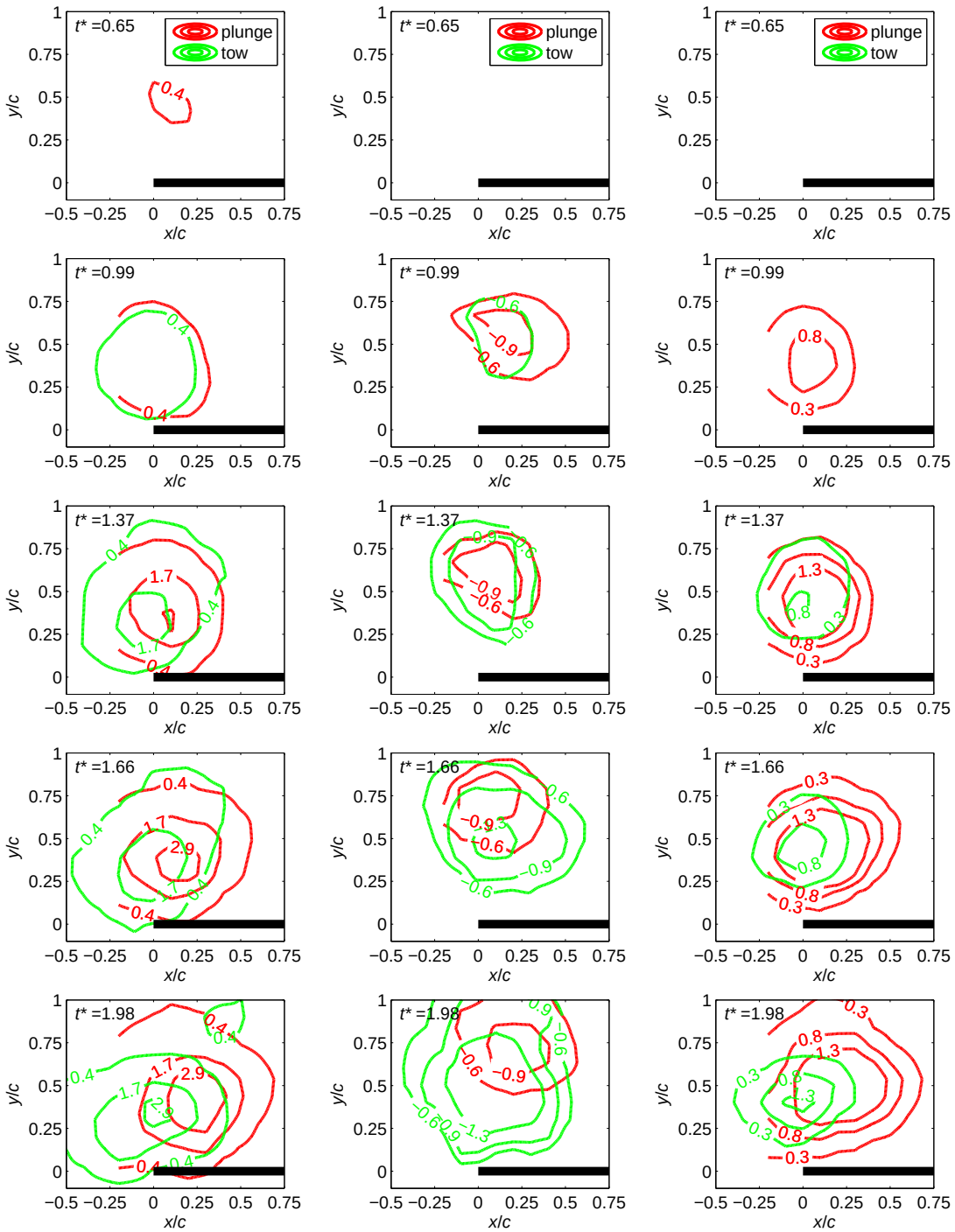

(a) spanwise vorticity ω_z^* (b) plate-normal acceleration a_y^{t*} (c) plate-normal vortex force L_y^*

Figure 8: Direct comparison of LEV results (XY-plane) in the near-midplane region ($1 \leq z/c \leq 3$): Isolines of (a) spanwise vorticity $\omega_z^* = \omega_z c/U_{\text{eff}}$; (b) plate-normal total acceleration $a_y^{t*} = a_y^t c/U_{\text{eff}}^2$; and (c) plate-normal component of the Lamb-vector $L_y^* = L_y c/U_{\text{eff}}^2$.

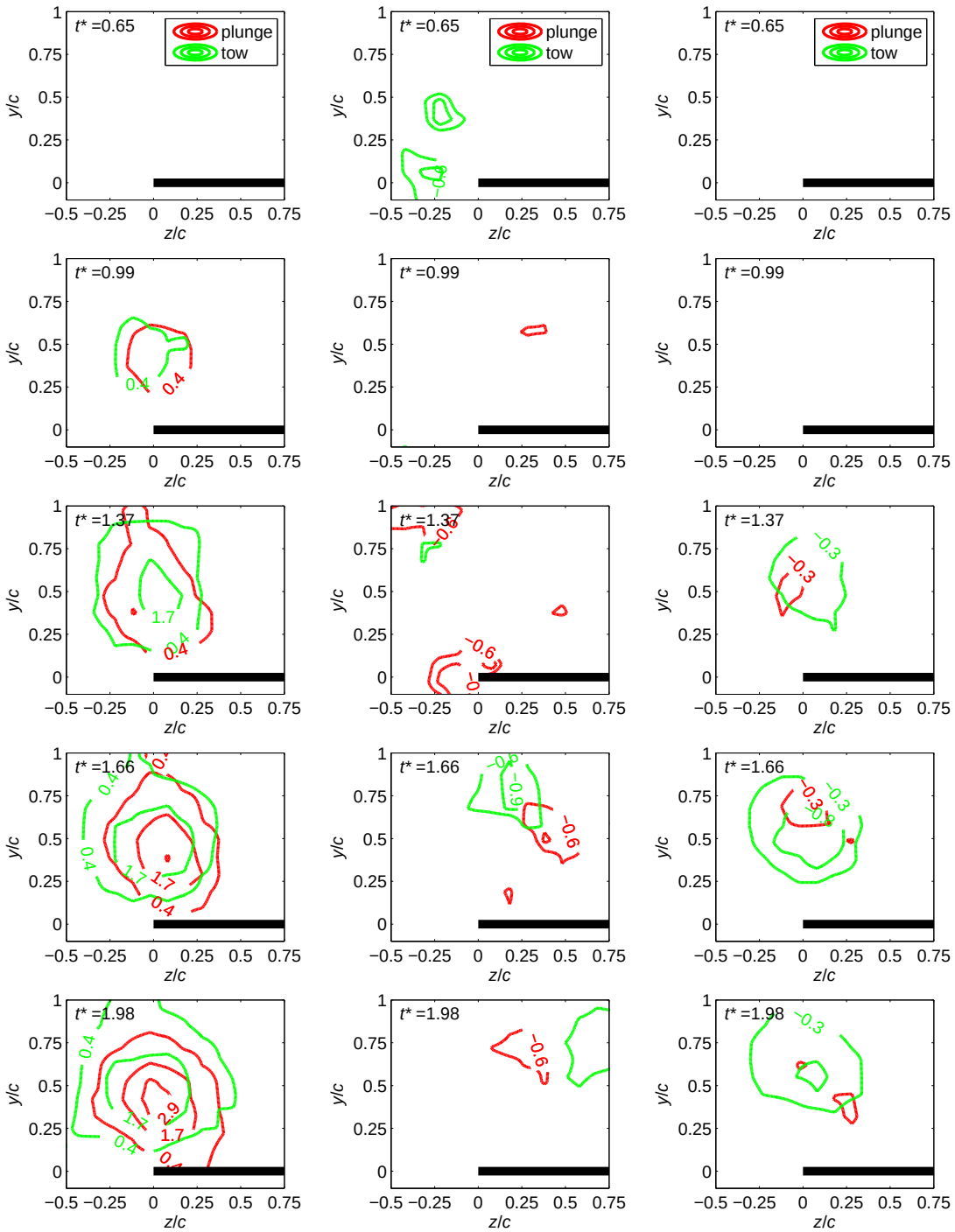

(a) streamwise vorticity ω_x^* (b) plate-normal acceleration a_y^{t*} (c) plate-normal vortex force L_y^*

Figure 9: Direct comparison of TV results (YZ-plane) in the near-tip region ($x/c = 0.6$): Isolines of (a) streamwise vorticity $\omega_x^* = \omega_x c/U_{\text{eff}}$; (b) plate-normal total acceleration $a_y^{t*} = a_y^t c/U_{\text{eff}}^2$; and (c) plate-normal component of the Lamb-vector $L_y^* = L_y c/U_{\text{eff}}^2$.

towing kinematics. This difference in total force was then studied via a rigorous analysis of the 3D-PTV data, i.e. direct comparison of vorticity, circulation, acceleration and vortex force. In particular, it has been demonstrated that a consideration of the integral circulation Γ_i oversimplifies the problem, i.e. identical spatio-temporal distributions of all three circulation components was observed along the plate's span. Furthermore, similar LEV formation for both kinematics was observed during rapid acceleration. Once this acceleration ceased, the tow LEV was observed to roll-off from the plate. It is hypothesized therefore that the inertia of the accelerated fluid in the vortical structure is responsible for this roll-off behaviour for $t^* \geq 1$. As a consequence, the development of vortex force was found to subside once the roll-off process started. Finally, the relative importance of the TV has been identified as a critical factor in the overall force production, particularly when significant amounts of spanwise (inboard) flow is observed. This insight is an important extension to the work of Ringuette *et al.* [9], where the key role of the TV was demonstrated for plate-normal kinematics, i.e. $\alpha_{\text{eff}} = 90°$. Here it can be concluded that the TV vortex force is affected by the magnitude of inboard-directed spanwise flow.

ACKNOWLEDGMENTS

The authors gratefully acknowledge funding from the Natural Sciences and Engineering Research Council of Canada.

REFERENCES

[1] J. O. Dabiri. On the estimation of swimming and flying forces from wake measurements. *Journal of Experimental Biology*, 208:3519–3532, 2005.

[2] Y. Feng, J. Goree, and B. Liu. Errors in Particle Tracking Velocimetry with High-Speed Cameras. *Review of Scientific Instruments*, 82:053707, 2011.

[3] S.I. Green. *Fluid Vortices: Fluid Mechanics and Its Applications*. Kluwer Academic Print on Demand, 1995.

[4] C. Hartloper, M. Kinzel, and D. Rival. On the Competition between Leading-Edge and Tip Vorticity for a Finite-Aspect-Ratio Pitching Plate. *Experiments in Fluids*, 54:1447, 2013.

[5] T. Jardin, A. Farcy, and L. David. Three-dimensional effects in hovering flapping flight. *Journal of Fluid Mechanics*, 702:102–125, 2012.

[6] D. Kim and M. Gharib. Flexibility Effects on Vortex Formation of Translating Plates. *Journal of Fluid Mechanics*, 677:255–271, 2011.

[7] J. Kriegseis, M. Kinzel, and D.E. Rival. On the persistence of memory: Do initial conditions impact vortex formation? *Journal of Fluid Mechanics*, (in revision).

[8] B. Lüthi, A. Tsinober, and W. Kinzelbach. Lagrangian Measurement of Vorticity Dynamics in Turbulent Flow. *Journal of Fluid Mechanics*, 528:87–118, 2005.

[9] M. J. Ringuette, M. Milano, and M. Gharib. Role of the Tip Vortex in the Force Generation of Low-Aspect-Ratio Normal Flat Plates. *Journal of Fluid Mechanics*, 581:453–468, 2007.

[10] P.G. Saffman. *Vortex Dynamics*. Cambridge Monographs on Mechanics and Applied Mathematics. Cambridge University Press, 1995.

[11] P. Sattari, D.E. Rival, R.J. Martinuzzi, and C. Tropea. Growth and Separation of a Start-Up Vortex from a Two-Dimensional Shear Layer. *Physics of Fluids*, 24:107102, 2012.

[12] G. D. Weymouth and M. S. Triantafyllou. Global vorticity shedding for a shrinking cylinder. *Journal of Fluid Mechanics*, 702:470–487, 2012.

[13] J.Z. Wu, H.Y. Ma, and J.Z. Zhou. *Vorticity and Vortex Dynamics*. Lecture notes in mathematics. Springer Berlin Heidelberg, 2005.

[14] T. O. Yilmaz and D. Rockwell. Flow Structure on Finite-Span Wings due to Pitch-Up Motion. *Journal of Fluid Mechanics*, 691:518–545, 2012.